Journal of Molecular Graphics and Modelling 44 (2013) 197–207

Contents lists available at ScienceDirect

Journal of Molecular Graphics and Modelling

journal homepage: www.elsevier.com/locate/JMGM

Structural and functional insights on folate receptor α (FRα) by homology modeling, ligand docking and molecular dynamics

Stefano Della-Longa [a,*], Alessandro Arcovito [b]

[a] Dipartimento di Medicina Clinica, Sanità Pubblica, Scienze della Vita e dell'Ambiente, Università dell'Aquila, Piazzale S. Tommasi 1, 67100, Coppito (AQ), Italy
[b] Istituto di Biochimica e Biochimica Clinica, Università Cattolica del Sacro Cuore, Largo F. Vito 1, 00168 Roma, Italy

ARTICLE INFO

Article history:
Accepted 31 May 2013
Available online 19 June 2013

Keywords:
Bioinformatics
Protein docking
Folate-targeted cancer therapies

ABSTRACT

Folate receptor α (FRα) is a cell surface, glycophosphatidylinositol (GPI)-anchored protein with a high affinity for its ligand partner, which is highly expressed in malignant cells and has been selected as a therapeutic target and marker for the diagnosis of cancer. No direct structural information is available from either X-ray diffraction or NMR on the post-translational structure of this disulfide-rich protein.

Three-dimensional models of the FRα structure have been derived with the recent homology modeling packages, using the crystal structure of the riboflavin-binding protein (RfBP) as a template. Molecular dynamics trajectories have been exploited allowing successfully the formation of a full disulfide bridge network, which was expected based on the similarities between FRα and RfBP. After the selection of the best model, a folic acid molecule was docked "in silico" onto the putative binding site and its binding mode was compared with that of vintafolide, a much larger molecule designed as a chemotherapy agent targeting specifically FRα. In both cases, a 40 ns molecular dynamics trajectory was calculated, providing suggestions regarding the key structural determinants driving the affinity and specificity of FRα for folic acid with respect to other folate homologues. Moreover, some other crucial experimental results related to the structure of the receptor are discussed, such as the expected location/accessibility of known immune epitopes, the set of N-linked glycosylation sites and the effect of point mutations on the impairment of folate binding. Our results may provide useful insights for studies related to folate-targeted drug delivery or cancer therapies involving folate uptake.

1. Introduction

Folate receptor α (FRα), also known as folate binding protein, LK26 trophoblastic antigen and GP38, is a membrane-bound glycoprotein of the folate receptor family, which includes the isoforms FRα, FRβ (72% identity) FRγ, (68% identity) [1]. Folate receptors are involved in the uptake and transport of various forms of the B-vitamin, folic acid. Dietary folic acid is taken up in the gut, metabolized in the liver to 5-methyltetrahydrofolate (5-MTHF) and subsequently distributed by the bloodstream. FRα is able to bind both folic acid and 5-MTHF with 0.34 and 1 nM affinity, respectively, and is expressed in many epithelial tissues, such as the choroid plexus, the retina and the placenta [2–5], whereas FRβ is expressed in the placenta and in hematopoietic cells, and FRγ in the spleen, the thymus, the bone marrow, and in ovarian and uterine carcinoma. Several features of FRα make it an attractive target for cancer immunotherapy: (i) It is largely shielded from the immune system in normal tissues; (ii) it becomes exposed when overexpressed on a variety of malignancies; and (iii) it is functionally active in cancer pathogenesis and is immunogenic. Many different immunotherapeutic methods targeting FRα are being explored to treat cancer [3]: passive immunotherapy includes monoclonal antibodies, antibodies modified to deliver treatments, and modified T cell therapy; active immunotherapy focuses on using FRα to increase the immunogenicity of cancer or to generate active FRα-directed immunity through a range of vaccination techniques. Finally, FRα has been selected as a target for anti-cancer drug delivery by specifically designed molecules, like vintafolide [6], or nanoparticle conjugates, including both the cancer drugs and folic acid as the targeting ligand [7].

According to the known sequence obtained from a cDNA library [8], there is a significant sequence similarity (Fig. 1A) between FRα and chicken riboflavin-binding protein (RfBP) [9–11]. In the region where the sequences clearly correspond, the sequence identity is more than 30%, indicating a structural and functional similarity between RfBP and FRα. Moreover, the sequence alignment of RfBP and FRα shows that the position of sixteen cysteines is conserved between the two proteins, strongly suggesting that the

* Corresponding author. Tel.: +39 0862433568
E-mail address: stefano.dellalonga@univaq.it (S. Della-Longa).

1093-3263/$ – see front matter © 2013 Elsevier Inc. All rights reserved.
http://dx.doi.org/10.1016/j.jmgm.2013.05.012

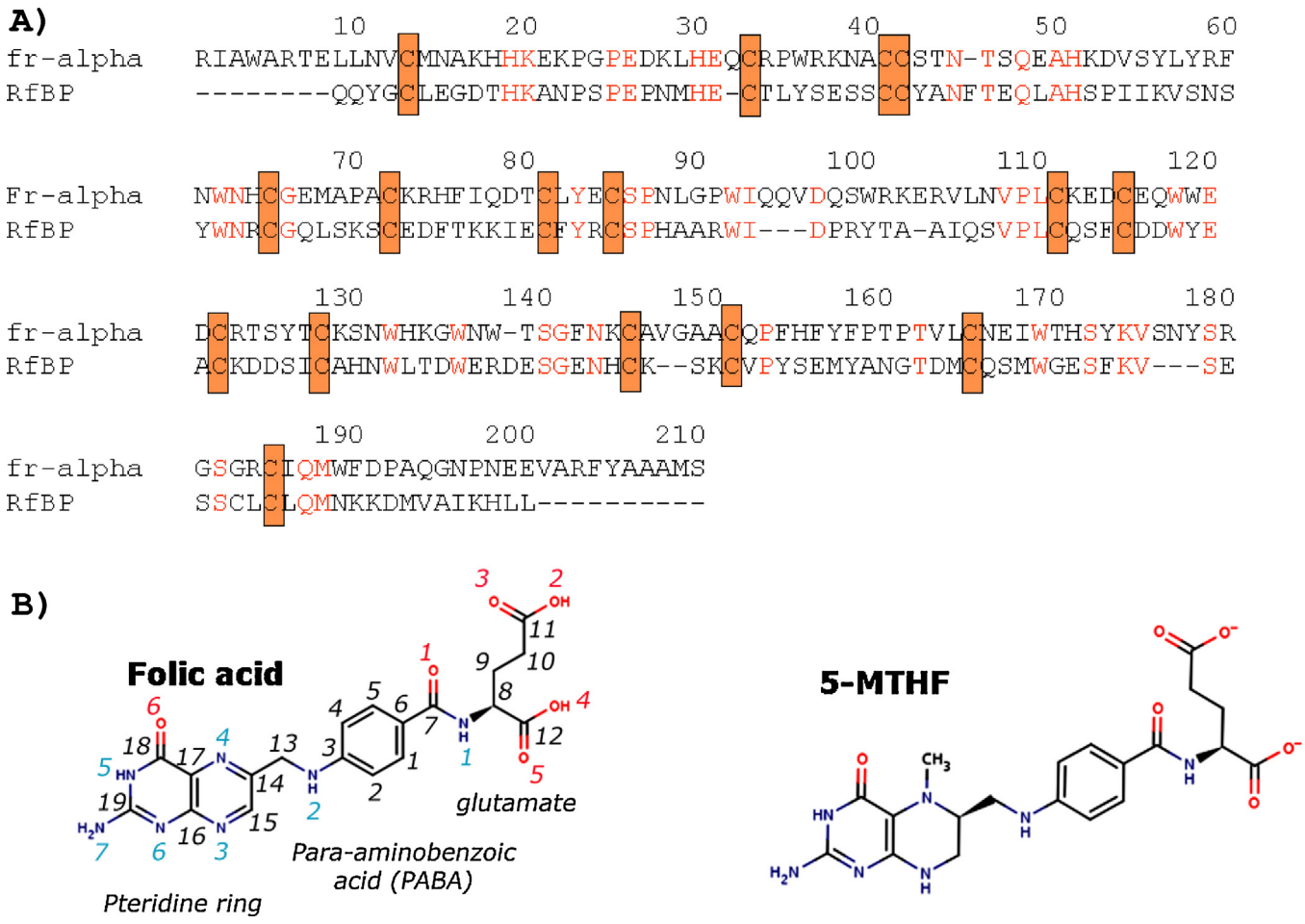

Fig. 1. (A) A CLUSTALW alignment between FRα and chicken RfBP, showing 27% identities, 49% positives, and the conserved positions of the 16 cysteine residues. (B) 2D image of folic acid (left) and 5-methyltetrahydrofolic acid (right). The numbering adopted in this work for the heavy atoms of folic acid is displayed.

bridging network formed by these eight disulfide bonds that has been found in the X-ray structure of RfBP may also be present in FRα [10]. Moreover, the RfBP structure shows that five out of the six tryptophans found in the sequence are clustered in the neighborhood of the ligand-binding site, stacking the riboflavin between the aromatic side chains of Trp156 and Tyr75. Relative to RfBP, FRα consists of a higher number of tryptophans, thirteen in FRα compared with six in RfBp, that are able to create a larger hydrophobic environment to accommodate the aromatic portion of folate. The two active forms of the B-vitamin that bind to FRα, folic acid and 5-methyltetrahydrofolate (5-MTHF), are depicted in Fig. 1B. Folic acid is composed of three primary structures: a hetero-bicyclic pteridine ring head, a central portion containing a para-aminobenzoic acid (PABA) and a glutamic acid end. The numbering used to identify each atom of folic acid is also reported. A homology model of the folate binding domain, based on the structure of the protein homologue RfBP, has already been proposed by Maziarz et al. [12] in an effort to identify the structural determinants associated with the primary sequence variations between FRα and FRβ receptors by site-directed mutagenesis. However this previously reported model was not analyzed in details and is not available. The aim of this study is to extend this homology model using recent modeling packages and to further investigate the FRα-folate complex "in silico". The results obtained are compared with known experimental evidence to shed light, at a molecular level, on this potentially interesting drug target for cancer therapies.

2. Methods

2.1. Modeling

The 257-amino-acid sequence of human FRα was chosen from a c-DNA library [8] (GenBank: AAB05827). The post-translational sequence of the protein was obtained by searching for signal sequences at the Signal Peptide Website (http://www.signalpeptide.de, ID 27557). The potential signal peptide (res. 1–24) is deleted, which has been confirmed in the bovine homologue (ID 29568), and the pro-peptide 235–257 is removed in the mature form to allow for the GPI anchor link to be arranged. A PSI-BLAST analysis of the final sequence revealed no homologous proteins with known 3D structures in the Protein Data Bank. However, the structure of the FRα homologue chicken riboflavin-binding protein (RfBP) has been reported in the literature [10], revealing the existence of 8 disulfide bridges, and its coordinates have kindly been delivered to us by the author (H. Monaco, personal communication). The CLUSTALW alignment between the mature FRα and RfBP sequences is shown in Fig. 1A, revealing 27% identity and 49% consensus similarity along the 210 residues. The positions of the 16 Cys residues are conserved between the two sequences; thus, it is expected that the disulfide bridge network of the two proteins will be identical. Under this assumption, the rather low homology between the proteins is counter-balanced by the existence of the constraints imposed by a disulfide bridge network, which strongly reduces the overall conformational space available.

According to this premise, and to build a model of FRα, the RfBP X-ray structure was chosen as a template, and the prediction of the 3D structure of the folate receptor was attempted by applying constraints on the S—S bond network.

One ab-initio modeling procedure, via the QUARK server [13], and three homology model procedures, the MODELLER [14], the SWISS-MODEL [15–17] and the I-TASSER servers [18,19], were chosen as described in Section 3.

2.2. Quality and refinement

The overall stereochemical quality of the 1–184 fragment of the X-ray structure of RfBP and the FRα "in silico" models was compared using the MOLPROBITY [20] analysis. In Table 1, the MOLPROBITY results are given for RfBP, FRα, and other representative disulfide rich proteins with known structures. MOLPROBITY added H atoms to the X-ray structure of RfBP and also detected some residues as being flipped (gln-2, gln-94, asn132, gln153 and gln171). Warnings were received during the geometric analysis, with the most severe warnings shown in bold italic and the less severe warnings shown in bold (see Table 1). The first warnings refer to rotamer outliers, Ramachandran favored regions, the Molprobity score, and bad angles.

To heed these warnings, the modeled structures were subjected to the "relax" protocol of the Rosetta suite package [21]. This protocol performs the structural refinement of a monomeric protein. It usually starts from a crude model, generated by a de novo structure prediction or homology modeling, and uses the Rosetta full-atom energy function to refine the structure while searching through conformational space. The protocol can dramatically lower the full-atom energy of a model, correcting local errors and improving interactions significantly by making relatively small adjustments to the protein backbone and side chain torsion angles from the starting structure.

The refined structures of the RfBP fragment and FRα were submitted to a further geometry check by MOLPROBITY and PROCHECK [22,23] analyses, revealing almost complete resolution of the initial problems (see Table 1 and Section 3).

2.3. Molecular dynamics

Classical molecular dynamics simulations of the FRα receptor in both the ligand-free and ligand-bound states (with folic acid and vintafolide) were performed using the GROMACS 4.5 package [24,25], testing different force fields in preliminary sessions, as explained in Section 3, to obtain a conformation with a full set of disulfide bridges. Thereafter, the GROMOS43A1 force field was adopted to compare the ligand-free and the ligand-bound dynamics. Ligand force fields were provided by the PRODRG program [26]. Charges and charge groups of the ligand were adjusted according to suggestions by Lemkul et al. [27]. The protein (or the protein–ligand complex) structure was solvated in a triclinic water box under periodic boundary conditions using a 1.0 nm minimum distance from the protein to the box faces and neutralizing the system using two Cl^- ions added to the solvent. The final systems consisted of approximately 25,000 atoms. Following the steepest descent minimization, the systems were equilibrated in the canonical ensemble (under NVT conditions for 100 ps at 300 K) and, subsequently, in the isothermal–isobaric ensemble (under NPT conditions for 100 ps), applying position restraints to the protein. Finally, all restraints were removed, and 40 ns molecular dynamics runs were performed under NPT conditions at 300 K. The temperature was maintained close to its reference value by applying the V-rescale [28] thermostat with a coupling constant of 0.1 ps. To maintain constant pressure (1 atm, isotropic coordinate scaling), the Parrinello–Rahman barostat [29] was used with a relaxation

Table 1
Quality assessment of our FR-α model, shown in comparison with other known structures from cystein rich proteins, according to the Molprobity analysis. The most severe and less severe warning are evidenced in bold italic and in bold, respectively. Within the percentile data, 100th percentile means the best among structures of comparable resolution, 0th means the worst.

	Analysis	Goal %	1BPI (1.09 Å) 3 S-S %	2E3 W (1.05 Å) 4 S-S %	1REX (1.5 Å) 4 S-S %	1B90 271 (1.65 Å) 4 S-S %	Rfbp fragment 184 (2.5 Å) 8 S-S %	Rfbp fragment (minimized structure)	FR-α (this work) 8 S-S
All atom contacts	Clashscore, all atoms (percentile)	>65th	**42nd**	79th	72nd	94th	***29.9th***	99th	97th
	Poor rotamers	<1	0	**1.8**	**2.8**	***6.6***	***10.2***	**3.9**	0
	Ramachandran outliers	<0.2	0	0	0	***0.6***	**0.5**	***1.1***	***1.6***
	Ramachandran favored	>98	98.2	97.6	100	***94***	***92.3***	***92***	***88***
	Cβ deviation > 0.25 Å	0	0	**1**	0	**4**	**8**	**2**	**4**
	Molprobity score (percentile)	–	75th	***65th***	***60th***	68th	***16th***	81th	88th
	Residues with bad bonds	0	***3.45***	0	0	0	0	0	0
	Residues with bad angles	<0.1	***1.72***	0	**1.5**	***3.7***	***1.1***	0	***8***

time of 2.0 ps. Van der Waals interactions were modeled using 6–12 Lennard–Jones potentials with a 1.4 nm cutoff. Long-range electrostatic interactions were calculated using the PME method, with a cutoff for the real space term of 0.9 nm. Covalent bonds were constrained using the LINCS algorithm. The time step employed was 2 fs, and the coordinates were saved every 2 ps for analysis, which was performed using the standard GROMACS tools.

2.4. Ligand docking

Docking of either folic acid or vintafolide to FRα was attempted. The vintafolide molecule was chosen to extend the present work, because in spite of its larger dimensions, it was designed to specifically target the toxic vinblastine group to cancer cells that overexpress the folic acid receptor [6].

According to the Autodock Vina 1.1 [29,30] software package, binding modes within a 30 Å × 30 Å × 30 Å box around the center of the putative binding pocket of FRα were generated; polar hydrogens were added by using the Hydrogens module in the AutoDockTools (ADT) program [31], and Gasteiger partial charges were assigned [32]. The Vina parameter "Exhaustiveness" was set to the value of 300. All other parameters were used at their default values. All rotatable bonds within the folic acid ligand, and the folic acid moiety of vintafolide, including the amide bond between PABA and glutamate, were allowed to rotate freely, whereas the receptor was considered rigid. Two-dimensional representations of the docking results for acid folic were produced using LIGPLOT [33].

3. Results

3.1. Model build-up

An ab-initio "in silico" design of the protein was attempted by submitting the post-translational fragment of FRα as the query sequence to the QUARK server [13] for a completely automated structure prediction procedure. QUARK models are built from small fragments (1–20 residues long) by replica-exchange Monte Carlo simulations under the guide of an atomic-level knowledge-based force field. Because no global template information is used in a QUARK simulation, the server is suitable for proteins that have no homologous templates. The best QUARK model is displayed in Fig. 2, together with the other predicted structures obtained by homology modeling and their template structure, from RfBP [10]. The QUARK procedures allow for the restraint of distances between cysteines implied by disulfide bonds; nevertheless, at the end of the procedure, we could not obtain reasonable bridge contacts, with the constrained S–S distances ranging from 2.98 to 8.31 Å.

As a second step, we used the X-ray structure of RfBP, kindly supplied by the author [10], as a template. Three homology modeling procedures were compared, according to the MODELLER [14], SWISS-MODEL [15–17] and I-TASSER servers [18,19].

MODELLER is a program for comparative protein modeling that satisfies spatial restraints. The models have good stereochemistry and are at least as similar to the crystallographic structures as the closest template structures. The largest errors occur in the regions that are not aligned correctly or where the template structures are not similar to the correct structure. These regions correspond predominantly to exposed loops, insertions of any length, and non-conserved side chains. The best model of FRα from MODELLER maintained 7 of the 8 expected S—S bonds, based on the FRα-RfBP alignment, but the disulfide bridge Cys128-Cys145 was not formed.

The SWISS-MODEL server was used in Project-mode. The Project file contained the RfBP template structure and the alignment between FRα and the template. From the output of this procedure, we obtained a 9–200 residue fragment that overlaps with the RfBP sequence. Likewise the case with MODELLER, all of the expected S—S bonds were formed apart the bond between Cys128 and Cys145. Hence, the same disulfide bridge is missing in both the MODELLER and SWISS-MODEL structures, suggesting that either there are some limitations to the actual threading algorithms when searching for the conformational minima of poorly conserved loops, or the conformation of the 135–151 loop favoring this S—S bond has much higher energy than that found "in silico".

MUSTER [19], included in the I-TASSER server [18], performs homology modeling either using the RfBP X-ray structure as a template or by protein threading, which is used to model those proteins that have the same folding patterns as proteins with known structures but do not have homologous proteins with known structures. The best I-TASSER model for FRα was obtained through homology modeling, for which we obtained a C-score value of −0.77, while values of less than −2 were obtained for the alternative models found by protein threading. The I-TASSER server allows for the inclusion of disulfide bridge restraints; nevertheless, the final model was found to have formed only one disulfide bridge.

The RMSD difference between each of the three homology models and the RfBP template has been calculated by first creating a pairwise sequence alignment according to the Needleman–Wunsch algorithm [34], using a BLOSUM-62 substitution matrix, and then superimposing the structures according to the pairwise alignment. The values obtained were 0.94 Å for MODELLER, 1.14 Å for I-TASSER, and 0.79 for Å SWISS-MODEL, between 140 atom pairs.

3.2. Refinement

The best models chosen by the MODELLER, SWISS-MODEL and I-TASSER servers were subjected to the ROSETTA-relax energy procedure, and the quality of the resulting structures was checked by the Prosa-web, MOLPROBITY and PROCHECK analyses. The MOLPROBITY quality indexes of the relaxed structures of RfBP and FRα (SWISS-MODEL) are illustrated in Table 1, together with the parameters related to the X-ray structures of other disulfide-rich proteins reported in the Protein Data Bank at a different resolution. From the MODELLER model, we obtained 92% of Ramachandran favored residues (vs. 92% and 87% for SWISS-MODEL and I-TASSER models, respectively), 0.96% of outliers (vs. 1.74% and 4.81%), and 84% of the MOLPROBITY clash-score rating (vs. 82% and 55%). On the basis of this result, we decided to further investigate only the structures obtained by MODELLER and SWISS-MODEL. Indeed, even though the quality indexes for the two models were comparable, the topology found was slightly different. Moreover, both models were able to construct all but the last of the 8 disulfide bridges that are expected to exist in the functional form of the receptor.

To find conformations compatible with a complete application of the disulfide bridge constraints, classical molecular dynamics simulations of the FRα receptor were followed, starting from the MODELLER and SWISS-MODEL structures, using the GROMACS 4.5 package [24,25]. First, the structures resulting from the homology modeling procedures were equilibrated in a water solvent as described in the Methods. Then, small trajectories (2–5 ns) were calculated using different force fields (CHARMM27, AMBER99SB, and GROMOS43a1). These short trajectories were investigated for any fast conformational changes that led to a minimal distance between Cys128 SG and Cys145 SG. Transient, short-lived conformations with smaller values of this distance were observed regardless of the force field adopted; however, when starting from the SWISS-MODEL structure (9–200 residue fragment) and using the AMBER99SB force field, the separation between the two sulfurs dropped from approximately 12 Å to approximately 4 Å in less than 1 ns, remaining stable along the trajectory duration (5 ns). Hence, a conformation was chosen from a single frame of this

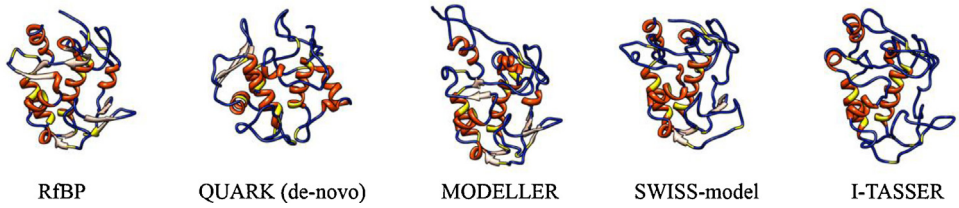

Fig. 2. From left to right: the X-ray structure of RfBP, segment 1–184 [10]; the predicted 3D structure of FRα based on a de-novo algorithm by QUARK; and three predicted structures obtained by homology modeling with protein threading starting from the RfBP protein structure template, according to the MODELLER, SWISS-MODEL, and I-TASSER packages. The α and β secondary structure segments are depicted in red and pink, respectively, and the loops are in blue. The 16 conserved cysteines involved in 8 disulfide bridges in RfBP are depicted in yellow. Images were obtained by the Chimera software [50].

trajectory, the last disulfide bridge constraint was applied, and the system was re-equilibrated as described in the Methods. Finally, the ROSETTA-relax protocol was applied to solve the residual local energy troubles. The resulting structure included the expected full network of 8 disulfide bridges, good quality indexes (Table 1, last column), and a clearly formed hydrophobic pocket; thus, this structure was used for ligand docking calculations. In the following section, we will briefly describe the structural features of the modeled structure that constituted our final model of the FRα receptor.

A sketch of the protein structure (yellow), superimposed to that of RfBP (blue), is represented in Fig. 3A. In Fig. 3B, a map of the FRα conserved residues within the folate receptor family (including other mammalian folate receptors α, β **γ**, and RfBP proteins) are shown; side chains of the highly conserved cysteins are displayed in red. The quality of the predicted SWISS-MODEL structure of the FRα receptor, according to the Prosa-web [35,36] analysis, is shown in Fig. 3C and D. According to this analysis, the overall model quality parameter of our model has a *z*-score of −6.31 (Fig. 3C). The *z*-score value is displayed in a plot that contains all of the experimentally determined protein chains in the current PDB from different sources (X-ray, NMR) to check whether the *z*-score of the input structure is within the range of scores typically found for native proteins of similar size. As is evident from Fig. 3C, the quality score is well within the score range corresponding to experimentally known structures for proteins of a similar size. Moreover, a local model quality index, displayed in Fig. 3D, was obtained by plotting the knowledge-based energy score as a function of amino acid sequence. In general, positive values correspond to problematic or erroneous sections of the input structure. A plot of single residue energies usually contains large fluctuations and is of limited value for model evaluations. Hence, the plot is smoothed by calculating the average energy over each 40-residue fragment s(i,i + 39), which is then assigned to the 'central' residue of the fragment at position i + 19 (thick line). A second line plotting the average energy over a smaller, 10-residue fragment is shown in the background of the plot (thin line). The 10-residue energies are positive only in the loop 90–110, i.e., around the β3β4 sheet; however it is known that

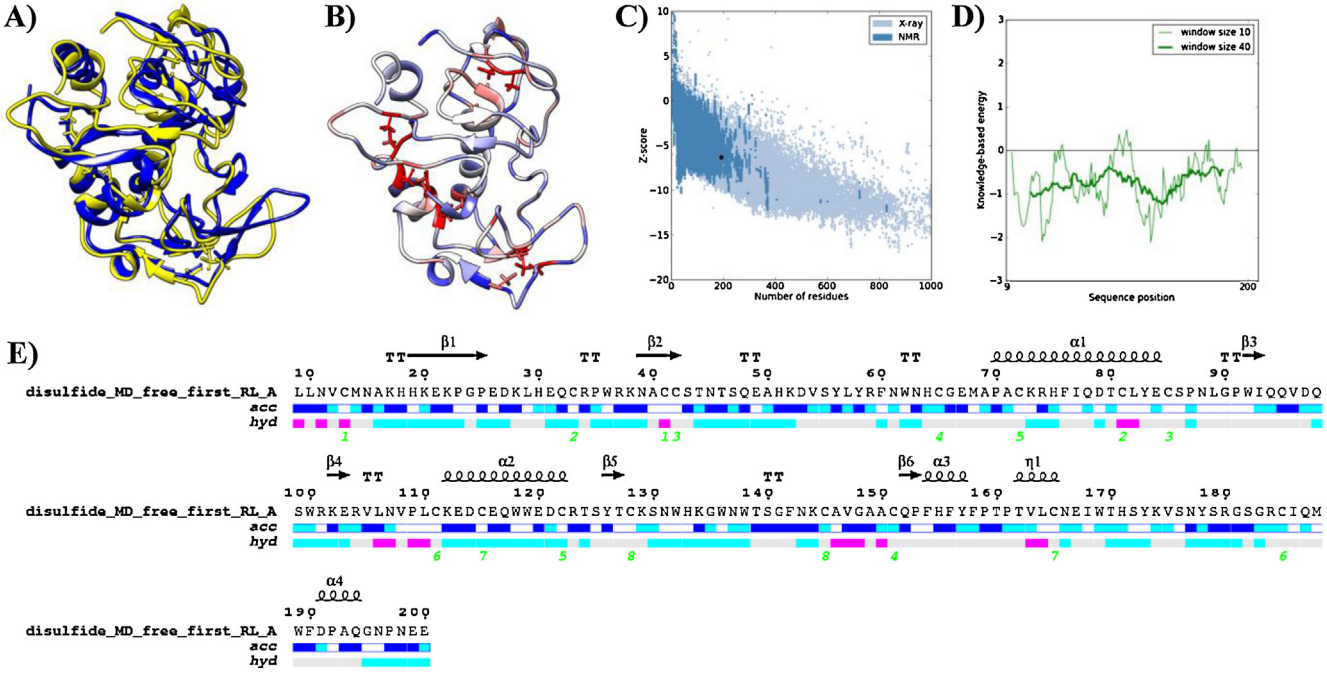

Fig. 3. (A) Superimposition of the structure of RfBP (blue) and FRα (SWISS-model, yellow). (B) Conservation map of the residues of Frα. The residue-conservation color code was obtained according to the multiple alignment of selected sequences within the Folate receptor family. More conserved residues are in red, less conserved residued are in blue. The side chains from the highly conserved cysteines are displayed. (C) Overall model quality according to Prosa-web [24,25], *z*-score = −6.31. (D) Local model quality according to Prosa-web. Energy values are plotted as a function of amino acid sequence. The plot is smoothed by calculating the average energy over each 40-residue fragment s(i,i + 39), which is then assigned to the 'central' residue of the fragment at position i + 19 (thick line). A second line with a smaller window size of 10 residues is shown in the background of the plot (thin line). (E) Secondary structure of FRα, including accessibility and hydropathy markers for each residue (from the ENDSCRIPT program: relative accessibility is shown below sequence by a blue-colored bar. A second bar gives the figure of hydropathy (red: hydrophobic, cyano: hydrophilic). (For interpretation of the references to colour in this figure legend, the reader is referred to the web version of this article.)

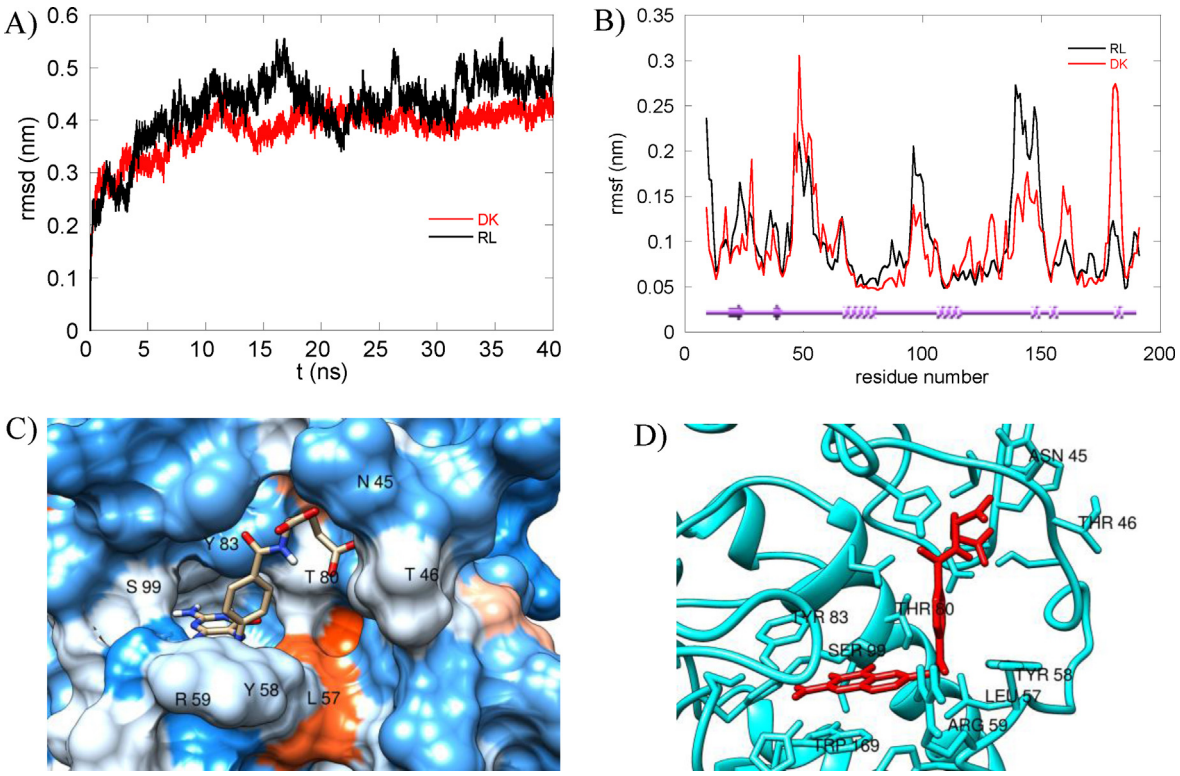

Fig. 4. (A) The RMSD trajectory (40 ns) of the ligand-free, Rosetta-relaxed receptor (RL, black line), and of the ligand-bound receptor, starting from the docking pose of folate to ligand-free FRα (DK, red line). (B) Residue-based RMSF of the ligand-free (RL, black line) and ligand-bound (DK) receptor. The location of α and β secondary structures is sketched (purple) at the bottom of the frame for clarity. (C) The docked structure. Surface contacts in the predicted docking site of folic acid on FRα. (D) The docked structure. Some residues linked by hydrophobic interactions or H-bond interactions to folic acid are labeled. (For interpretation of the references to colour in this figure legend, the reader is referred to the web version of this article.)

the Prosa-web analysis of many X-ray structures in the PDB with resolution lower than 1.5 Å show such local positives of the 10-residue energies. On the other hand the energies remain negative throughout the sequence in the 40-residue average. In particular, the region involved in the 128–145 disulfide bridge constraint does not show any energy troubles.

3.3. Predicted structure of FRα

It is evident from the superimposition of the structures of RfBP and the SWISS-MODEL (Fig. 3A) that the overall secondary structure of RfBP is well reproduced in FRα, apart from a β-sheet that is present in RfBP, but is absent in the SWISS-MODEL structure (135–151 loop), likely due to differences (insertions and variations) between the primary sequences.

A more detailed description of the secondary structure of FRα (Fig. 3E), including accessibility and hydropathy markers for each residue, was obtained by the ENDSCRIPT program of the ESPRIT package [37]; the relative accessibility is enlightened below the sequence by a blue bar. A second bar gives the figure of hydropathy (red: hydrophobic, cyan: hydrophilic), calculated from the sequence according to the Kyte–Doolittle algorithm [38]

As displayed in Fig. 3E, Asn45, Asn137 and Asn177 are well accessible to N-linked glycosylation; the latter two glycosylation sites have been identified experimentally [39], while the site at Asn45 is based on similarity to other glycosylation sites in the UNIPROTK database (entry P15328). However, according to our structure, Asn45 is located at the entrance of the hydrophobic pocket that has been identified as the putative binding site, discouraging its involvement in post translational modifications, as illustrated in the next section.

3.4. Docking and dynamics of FRα

According to the protocol described in Section 2, flexible-ligand docking of folic acid to the FRα structure (Rosetta-relaxed SWISS-MODEL with 8 disulfide bonds) was attempted by the Autodock-Vina 1.1 procedure. All rotatable bonds of the folate, including the amide bond between the glutamate moiety and the PABA ring, were considered. At the end of the procedure, 9 docking poses were obtained, with predicted binding affinity values between −9.5 and −8.8 Kcal/mol and with different orientations and configurations of the folate. To select a functionally relevant docking conformation, we choose a pose with a binding affinity of −8.8 Kcal/mol, with the pteridine ring buried inside the hydrophobic pocket and the glutamic end close to the external side. This orientation allows the binding of folate conjugates with even larger moieties linked to the glutamate end, in agreement with the known ability of this receptor to bind larger molecules, including vintafolide, with high affinity. This last compound is a derivative of the anti-mitotic chemotherapy drug vinblastine, which is chemically linked to folic acid [40]. The vintafolide molecule was designed to specifically target the toxic vinblastine group to cancer cells that overexpress FRα. As we will show below, the “in silico” docking of folic acid and vintafolide to FRα is obtained with similar geometric features.

A blow-up of the resulting structure of the receptor and the docked folate molecule, centered on the docking site, is displayed in Fig. 4C and D, where the residues interacting with the ligand are labeled. According to the atom nomenclature used for folate as indicated in Fig. 1B, an interaction diagram of the receptor–ligand complex achieved by Autodock-Vina docking was obtained using LIGPLOT [33], as shown in Fig. 5. Accordingly, the PABA-pteridine

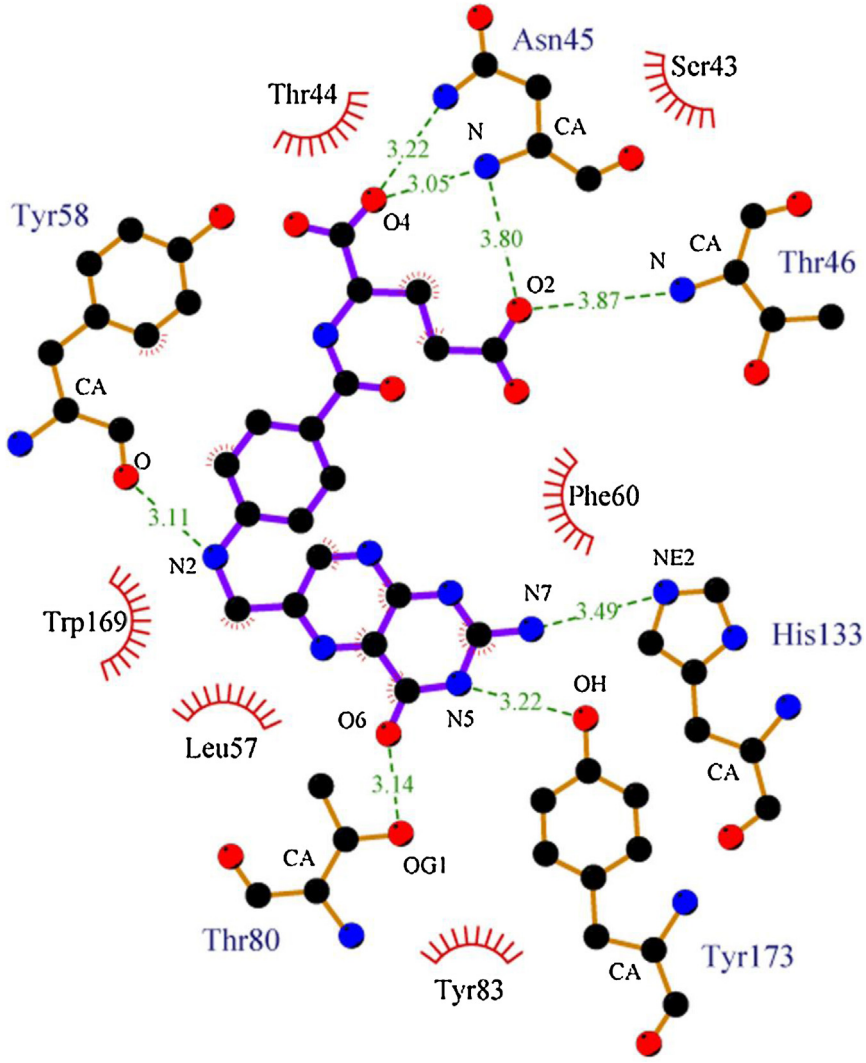

Fig. 5. 2D interaction diagram of the predicted Frα-folate complex (from LIGPLOT software).

moiety of folic acid is buried in a hydrophobic core formed by Leu57, Phe60, Tyr83 and Trp169, its pteridine ring head stacked between the Trp169 and Tyr83 aromatic rings; this hydrophobic environment further includes a surrounding set of conserved Trp residues, i.e., 62, 92, 118, 132 and 135. The receptor-ligand interaction is then stabilized by H-bond interactions between the N5, N7 (donors), and O6 (acceptor) atoms of the pteridine ring of folate and Tyr173-OH, His133-NE2, and Thr80-OG1, respectively. Moreover, the N2 donor near the PABA ring is at a H-bond distance from the Tyr58-O. Furthermore, the H-bond interactions occur in proximity with the protein exterior, between the glutamic end (O4 and O2 acceptors) and the residues Asn45 and Thr46. According to this last result, the participation of Asn45 in N-linked glycosylation should impair folate binding; thus, the prediction can be made that Asn45 is not glycosylated in the mature functional protein. This prediction is in line with the experimental evidence from Picariello et al. [39], who reported glycosylation sites at the Asn137 and Asn177 positions but not at the Asn45 site.

A further insight into the degree of flexibility for FRα can be obtained from molecular dynamics. RMSD plots of the 40 ns MD trajectories of the Rosetta-relaxed, ligand-free receptor (RL, black line) and the ligand-bound receptor (starting from the docking pose to the ligand-free structure, DK, red line) are displayed in Fig. 4A, showing good stability and a certain degree of conformational relaxation of the ligand-free and ligand-bound structures. The residue-based Cα RMSF, relative to the average structure in the last 500 ps, is shown in Fig. 4B. The diagram shows a high degree of flexibility (particularly the 45–54, 95–104 and 136–150 fragments), as is expected by the high percentage of unstructured segments inside the sequence. Interestingly, the presence of the folate reduces the mobility of segments 95–104 and 136–150, which are involved in both hydrophobic and electrostatic interactions with folate, and increases the mobility of the 45–54 and 178–183 fragments. This latter fragment is closer to the C-terminal Ser; ligand-linked changes of conformation or dynamics involving this fragment could be related to the intracellular signaling pathways that involve the C-terminal ligated GPI anchor as a signal transducer [41]. However, no conclusion can be drawn in the absence of a more realistic model, including the receptor, the GPI anchor and a membrane fragment. The MD simulation run of the FRα-folate complex will be further discussed in the last part of the Results section.

Due to the large flexibility of the ligand-free receptor, interactions close to the receptor surface that involve the glutamate moiety of the ligand are expected to be less stable. Further suggestions about the binding properties of FRα come from affinity data as reported in literature or in the ZINC databank (http://zinc.docking.org) for folic acid (0.34 nM) and its related molecules. A list of these molecules includes antifolates

specifically targeted to FRα [42], as well as lometrexol (DDATHF, 0.43 nM), pemetrexed (0.28 nM), raltitrexed (0.55 nM) and ZD9331 (0.62 nM); a large group of folate homologues with measured affinity for FRα; and vintafolide (0.46 nM). The receptor can bind with nanomolar affinity these largely different folate ligands, with the glutamate moiety being the only chemical feature shared by all of them. This property suggests that these molecules dock inside the hydrophobic pocket with rather different arrangements, and is reasonable that, together with a large hydrophobic core able to accommodate different aromatic moieties, several different residues at the surface of the receptor, that are capable of H-bond interactions with glutamate, may be recruited for specific interaction with each one of the above mentioned homologues. The following section on the molecular dynamics of the receptor-ligand complex will be helpful to describe this situation. Indeed, largely extended hydrophobic interactions can drive and store the pteridine ring (as well as similar aromatic entities) inside the binding pocket, while other selected H-bonds may occur with each specific aromatic group; moreover, the internal groups of glutamate (N2 donor and O1, O4, and O5 acceptors) could further stabilize the bonds forming an H-bond network near the receptor surface. The remaining part of the ligand, if present, linked to the glutamic end, can be transported without any interactions, as should be the case of the long tail of vintafolide. Clearly, this ability to transport large cargoes inside the cell is of special interest, especially in light of cancer therapies using drug delivery by nanoparticles opportunely modified with a folate-targeting molecule.

3.5. *Predicted dynamics of the FRα-folate complex*

According to the docking procedure adopted, the FRα protein chain remains perfectly rigid. However, a readjustment of the binding pocket may be necessary for a more favorable binding interaction. As mentioned above, a certain degree of structural relaxation is observable when viewing the 40 ns RMSD plot of the FRα-folate complex. In Fig. 6A the time course of the distance between the pteridine ring and the Trp169 aromatic ring is visualized. As discussed above, the pteridine ring is stacked between Trp169 and Tyr83 aromatic rings. Due to the high flexibility of the receptor, a transient exit of the pteridine ring from this position is observed along the trajectory, followed by recovering of the initial conformation.

Secondly, and more importantly, MD simulations suggest that other residues aside from those revealed by the docking algorithm can be involved in the binding of the ligand, and also more residues can "take turns" at forming short-lived interactions with the same ligand atom to stabilize the main hydrophobic interaction occurring at the pteridine ring end. Along the 40 ns trajectory, the distances between several donor/acceptor atoms from receptor residues and the atoms O1, O4, O5 and N1 of folate fluctuate, showing short-lived minima representing possible transient electrostatic interactions beyond those observed by docking on a rigid protein environment. Specifically, we observe, at different times, short-lived minima for the following distances: Ser99(OG)-folate(O1), Lys134(NZ)-folate(O1), Gln98(NE2)-folate(O1) (see Fig. 6B); Ser140(OG)-folate(O4), Tyr58(OH)-folate(O4) (Fig. 6C); Ser99(OH)-folate(N1), Arg59(NE)-folate(O5), Ser140(OG)-folate(O5) and Tyr58(OH)-folate(O5) (not shown). The plots of Fig. 6B and C clearly show a relaxation of the system and a change of the residues involved in stabilizing the ligand binding. In particular, residues Ser99 and Glu98 are replaced by Lys34 in the interaction with folate (O1) (Fig. 6B). Moreover, the Tyr58(OH)-folate(O4) distance only at the very beginning of the molecular dynamics run (<1 ns) can be classified as forming electrostatic interaction, and Tyr58 is rapidly replaced by Ser140 (Fig. 6C). However the reliability of the results obtained by refining homology

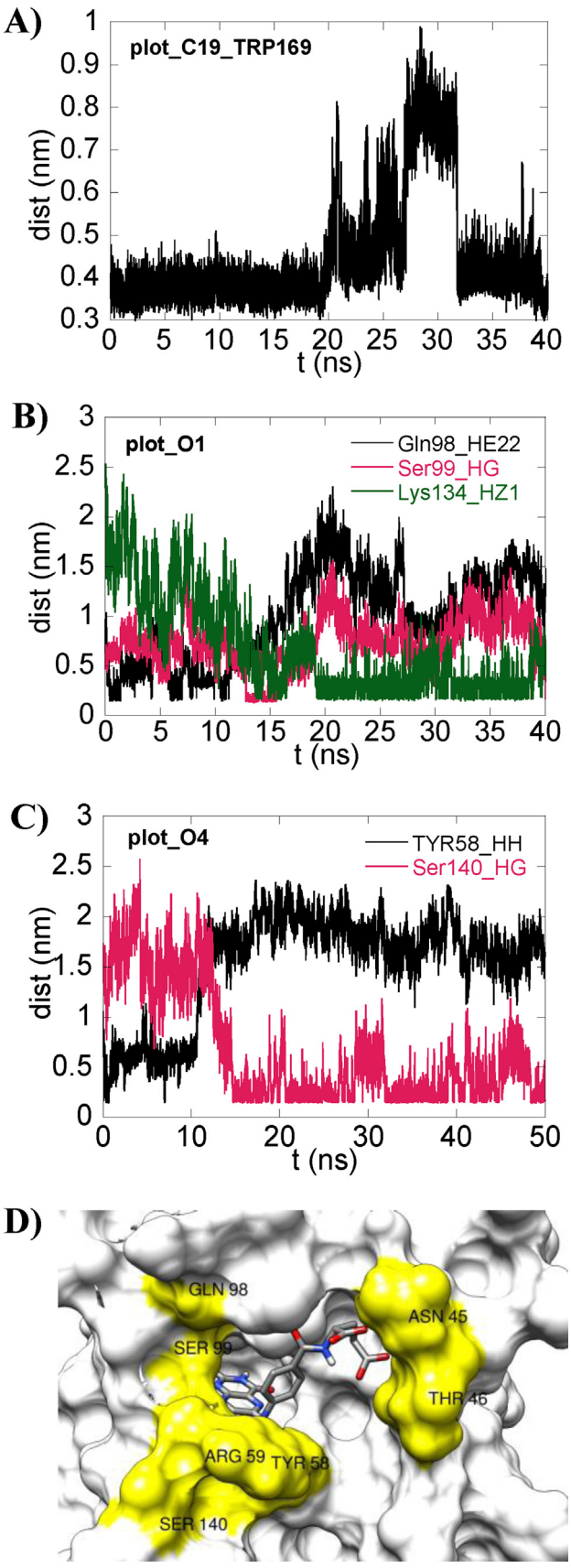

Fig. 6. (A) Time course of the distance between folate (C19) located on the pteridin ring, and TRP169((CZ3); (B) Time course of electrostatic interactions between folate(O1) and protein residues, as indicated in the legend; (C) Similar plot for folate(O4) and protein residues, as indicated in the legend; (D) Surface residues (yellow) of FRα able to interact with atoms O1, O4, O5 and N1 of the glutamate moiety of folate, during the MD simulation run of the receptor-ligand complex.

models using MD is still debated, as it has been shown in several test cases that that simulations initiated from homology modeling drift away from the native structure [43]. Thus the plots can be used for suggesting alternative partners for the exogenous ligands to the mentioned atoms, rather than describing the evolution of the protein complex system at such an high resolution.

Fig. 6D shows the localization of these residues (colored yellow) at the entrance of the ligand pocket. We speculate that they could act as a network of transiently formed stitches that take turns to stabilize the complex and are able to interact with a low specificity for molecules sharing the same glutamate moiety of the ligand. Similarly, the hydrophobic pocket should be flexible enough to accommodate 5-MTHF as well as folic acid with nanomolar affinity; indeed, the change in the protonation state as well as the methylation of N4 (pteridine ring), which together generate a rather distorted geometry for 5-MTHF when compared with folic acid, weakly perturb the hydrophobic environment surrounding the pteridine ring (Leu57, Phe60, Tyr83 and Trp169).

Last, we have applied the VINA docking algorithm and MD to qualitatively model the FRα-vintafolide complex that is known to form with 0.46 nM affinity. Due to the huge number of rotamers present in vintafolide (see Fig. 7A), only 32 of them (the maximum number acceptable from the VINA algorithm), located near the folate end of vintafolide, were let free to rotate. Fig. 7B shows how the hydrophobic pocket FRα is suited to dock vintafolide (yellow) as well as folic acid (red), by driving and storing the pteridine moiety inside, and leaving a large part of the molecule outside. A 40 ns MD trajectory of the FRα-vintafolide complex was then performed leaving all the rotamers of vintafolide free to rotate. Fig. 7C show the time course of the distance between the pteridin ring of vintafolide and the aromatic portion of Trp169; this distance remains nearly constant, thus demonstrating the stability of the complex "in silico".

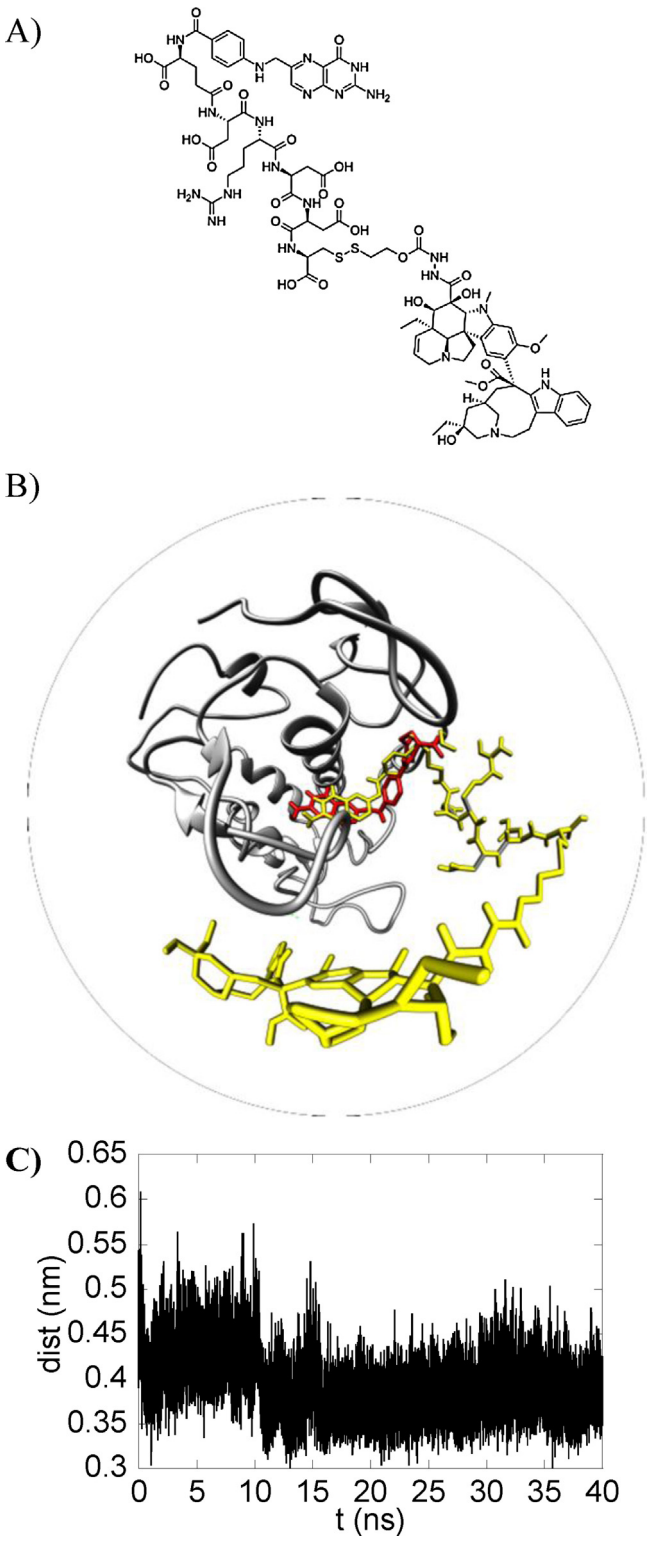

Fig. 7. (A) 2D diagram of vintafolide. (B) Dome view of the useful binding modes of either folate (red) or vintafolide (yellow) to Frα, superimposed after independent calculations carried out by the VINA docking algorithm. (C) Time course (40 ns) of the distance between the pteridin ring of vintafolide and Trp169 aromatic moiety. (For interpretation of the references to colour in this figure legend, the reader is referred to the web version of this article.)

4. Discussion

The prediction of the 3D structures of disulfide-rich proteins is a very difficult task due to the known complexity and diversity of their folding pathways [44]. Under the assumption that the conserved cysteine residues of the FRα and RfBP protein sequences correspond to a conserved disulfide bridging network, this task has been undertaken. Seven out of eight disulfide bridges were successfully reproduced in FRα by two homology modeling procedures, in spite of the rather low sequence identity between FRα and RfBP. The last S–S bridge was built as a constraint introduced in a favorable transient conformation of the receptor within a MD trajectory, just mimicking a final folding step. The development of new computational algorithms that can efficiently analyze the folding free energy landscapes of disulfide-rich polypeptides will be necessary to improve the present analysis; such an improvement would be of outstanding interest.

In the present paper, a possible structure of the ligand-binding pocket of FRα and of the folate-FRα complex has been derived. In spite of the actual limitations of bioinformatics tools [45] and the debated accuracy of molecular dynamics [46], our FRα structure accounts for some of the known experimental features of the receptor, i.e., the high accessibility of regions 96–100, 145–150 and 174–185 observed by hydrogen/deuterium (H/D)-exchange analyses [47] and the accessibility of Asn137 and Asn177 to N-glycosylation. Moreover, epitopes for monoclonal antibodies have been reported at regions 17–29, 45–57, 67–82 and 174–185 from the same authors [47]. According to our structure (Fig. 8), regions 17–29 (purple), 45–57 (red) and 174–185 (green) are well exposed to the solvent; however, region 67–82 (blue) is an α-helix segment that is less accessible, which has been experimentally confirmed by a very slow H/D-exchange rate. Region 67–82 (blue) is not in close proximity to region 174–185 (green), which is in apparent contrast with the measured competitive binding of their respective targeting monoclonal antibodies (mAb) [47]. However, the embedded

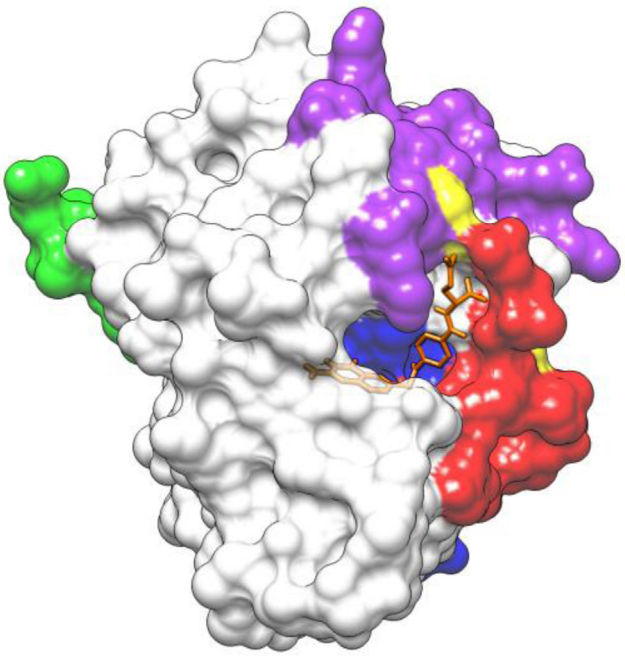

Fig. 8. A representation of the known mAb epitopes on the predicted FRα structure. Color code: blue–α-helix 67–82 (mAb 24F12); red–loop 45–57 (mAb MorAB003); green–loop 174–185 (mAb 26B3); and purple–loop 17–29 (mAb 9F3). Two residues involved in important point mutations are depicted in yellow: Ser 43, located at the entrance of the ligand-binding site; and Ala 50, just behind Asn 45 and Thr 46, which interact with the ligand. The other regions of the surface are in white. (For interpretation of the references to colour in this figure legend, the reader is referred to the web version of this article.)

localization of the 67–82 epitope suggests that any interaction between this region and its antibody could result in changes in the protein conformation affecting the binding of other mAbs that are conformationally oriented on locations not necessarily in close proximity to the 67–82 epitope.

A satisfactory model of FRα should be able to explain the effects of point mutations that impair the binding of folate. At least one known point mutation, Ser43Pro, results in the full impairment of folate binding [48]. According to our "in silico" model, Ser43 resides in a crucial location, in close proximity with two interacting residues (Asn45 and Thr46) and with two disulfide bridges involving its nearest neighbors, Cys41 and Cys42. Thus, it is very likely that the Ser43Pro mutation results in a strong rearrangement of the tertiary structure just around the hydrophobic pocket, explaining the severe impairment of its binding properties.

A more challenging task would be to clarify the roles of specific amino acid substitutions that are able to affect the affinity features of FRα and its closely related isoforms, FRβ and FRγ, which is greatly relevant in the research fields of drug delivery, (immuno) therapy and cancer diagnostics. Some mutations (Ala50Leu, Val105Phe and Glu166Gly) have been reported to result in a differential ligand-binding affinity between FRα and FRβ [12], and Ala50Leu has been shown to be responsible for functional divergence, resulting in FRβ having a different affinity and an opposite stereospecificity for 5-MTHF and folic acid isomers when compared with FRα. According to our structure, Ala50 is located just behind Asn45 and Thr46; thus, the Ala50Leu point mutation could be able to affect folate affinity, whereas no clear indications can be assumed from the positions of the other two mutations, which occur on residues located far from the binding site.

Finally, at least one example has been reported of a reduced and alkylated form of folate that binds FRα but not FRβ [49]. Unfortunately, in the absence of any experimental data from X-ray diffraction or NMR, the "in silico" explanation of the functional diversity between FRα and FRβ, involving a comparison of two predicted structures and their complexes with ligands, seems to be a goal whose required accuracy is far beyond that provided by this homology model. Notwithstanding all of the underlined limitations of our "in silico" approach, we believe that the present study can be helpful for stimulating further experimental research of FRα.

Acknowledgments

Financial support by the Italian Ministry of University and Research [Linea D1 Università Cattolica Sacro Cuore] is gratefully acknowledged. Thanks are due to Prof. H. Monaco for providing the crystallographic coordinates of RfBP to us.

References

[1] A.C. Antony, The biological chemistry of folate receptors, Blood 79 (1992) 2807–2820.
[2] C.D. Chancy, R. Kekuda, W. Huang, P.D. Prasad, J.M. Kuhnel, F.M. Sirotnak, P. Roon, V. Ganapathy, S.B. Smith, Expression and differential polarization of the reduced-folate transporter-1 and the folate receptor alpha in mammalian retinal pigment epithelium, Journal of Biological Chemistry 275 (2000) 20676–20684.
[3] G.T. Clifton, A.K. Sears, K.S. Clive, J.P. Holmes, E.A. Mittendorf, C.G. Ioannides, S. Ponniah, G.E. Peoples, Folate receptor alpha: a storied past and promising future in immunotherapy, Human Vaccines 7 (2011) 183–190.
[4] N. Solanky, A. Requena Jimenez, S.W. D'Souza, C.P. Sibley, J.D. Glazier, Expression of folate transporters in human placenta and implications for homocysteine metabolism, Placenta 31 (2010) 134–143.
[5] S.D. Weitman, R.H. Lark, L.R. Coney, D.W. Fort, V. Frasca, V.R. Zurawski Jr., B.A. Kamen, Distribution of the folate receptor GP38 in normal and malignant cell lines and tissues, Cancer Research 52 (1992) 3396–3401.
[6] F. Dosio, P. Milla, L. Cattel, EC-145, a folate-targeted vinca alkaloid conjugates for the potential treatment of folate receptor-expressing cancers, Current Opinion in Investigational Drugs 11 (2010) 1424–1433.
[7] J.H. Maeng, D.H. Lee, K.H. Jung, Y.H. Bae, I.S. Park, S. Jeong, Y.S. Jeon, C.K. Shim, W. Kim, J. Kim, J. Lee, Y.M. Lee, J.H. Kim, W.H. Kim, Biomaterials 31 (2010) 4995–5006.
[8] S.W. Lacey, J.M. Sanders, K.G. Rothberg, R.G. Anderson, B.A. Kamen, Complementary DNA for the folate binding protein correctly predicts anchoring to the membrane by glycosyl-phosphatidylinositol, Journal of Clinical Investigation 84 (1989) 715–720.
[9] L. Nygren-Babol, M. Jagerstad, Folate-binding protein in milk: a review of biochemistry, physiology, and analytical methods, Critical Reviews in Food Science and Nutrition 52 (2011) 410–425.
[10] H.L. Monaco, Crystal structure of chicken riboflavin-binding protein, Embo Journal 16 (1997) 1475–1483.
[11] D.B. Zheng, H.M. Lim, J.J. Pene, H.B. White 3rd., Chicken riboflavin-binding protein. cDNA sequence and homology with milk folate-binding protein, Journal of Biological Chemistry 263 (1988) 11126–11129.
[12] K.M. Maziarz, H.L. Monaco, F. Shen, M. Ratnam, Complete mapping of divergent amino acids responsible for differential ligand binding of folate receptors alpha and beta, Journal of Biological Chemistry 274 (1999) 11086–11091.
[13] D. Xu, Y. Zhang, Ab initio protein structure assembly using continuous structure fragments and optimized knowledge-based force field, Proteins 80 (2012) 1715–1735.
[14] A. Sali, L. Potterton, F. Yuan, H. van Vlijmen, M. Karplus, Evaluation of comparative protein modelling by MODELLER, Proteins 23 (1995) 318–326.
[15] K. Arnold, L. Bordoli, J. Kopp, T. Schwede, The SWISS-MODEL workspace: a web-based environment for protein structure homology modelling, Bioinformatics 22 (2006) 195–201.
[16] F. Kiefer, K. Arnold, M. Kunzli, L. Bordoli, T. Schwede, The SWISS-MODEL Repository and associated resources, Nucleic acids Research 37 (2009) D387–D392.
[17] M.C. Peitsch, Protein modeling by E-mail, Biotechnology 13 (1995) 658–660.
[18] A. Roy, A. Kucukural, Y. Zhang, I-TASSER: a unified platform for automated protein structure and function prediction, Nature Protocols 5 (2010) 725–738.
[19] S. Wu, Y. Zhang, MUSTER: Improving protein sequence profile-profile alignments by using multiple sources of structure information, Proteins 72 (2008) 547–556.
[20] V.B. Chen, W.B. Arendall 3rd, J.J. Headd, D.A. Keedy, R.M. Immormino, G.J. Kapral, L.W. Murray, J.S. Richardson, D.C. Richardson, MolProbity: all-atom structure validation for macromolecular crystallography, Acta Crystallographica. Section D Biological Crystallography 66 (2010) 12–21.
[21] K.W. Kaufmann, G.H. Lemmon, S.L. Deluca, J.H. Sheehan, J. Meiler, Practically useful: what the Rosetta protein modeling suite can do for you, Biochemistry 49 (2010) 2987–2998.
[22] R.A. Laskowski, PDBsum new things, Nucleic Acids Research 37 (2009) D355–D359.

[23] R.A. Laskowski, E.G. Hutchinson, A.D. Michie, A.C. Wallace, M.L. Jones, J.M. Thornton, PDBsum: a web-based database of summaries and analyses of all PDB structures, Trends in Biochemical Sciences 22 (1997) 488–490.
[24] H.J.C. Berendsen, D. van der Spoel, R. van Drunen, GROMACS: a message-passing parallel molecular dynamics implementation, Computer Physics Communications 91 (1995) 43–56.
[25] B. Hess, C. Kutzner, E. Lindhal, GROMACS 4: algorithms for highly efficient, load-balanced, and scalable molecular simulation, Journal of Chemical Theory and Computation 4 (2008) 435–447.
[26] A.W. Schuttelkopf, D.M. van Aalten, PRODRG: a tool for high-throughput crystallography of protein-ligand complexes, Acta Crystallographica. Section D Biological Crystallography 60 (2004) 1355–1363.
[27] J.A. Lemkul, W.J. Allen, D.R. Bevan, Practical considerations for building GROMOS-compatible small-molecule topologies, Journal of Chemical Information and Modeling 50 (2010) 2221–2235.
[28] G. Bussi, D. Donadio, M. Parrinello, Canonical sampling through velocity rescaling, Journal of Chemical Physics 126 (2007) 014101.
[29] M. Parrinello, A. Rahman, Polymorphic transitions in single crystals: a new molecular dynamics method, Journal of Applied Physics 52 (1981) 7182–7190.
[30] O. Trott, A.J. Olson, AutoDock Vina: improving the speed and accuracy of docking with a new scoring function, efficient optimization, and multithreading, Journal of Computational Chemistry 31 (2010) 455–461.
[31] G.M. Morris, R. Huey, W. Lindstrom, M.F. Sanner, R.K. Belew, D.S. Goodsell, A.J. Olson, AutoDock4 and AutoDockTools4: automated docking with selective receptor flexibility, Journal of Computational Chemistry 30 (2009) 2785–2791.
[32] J. Gasteiger, M. Marsili, Iterative partial equalization of orbital electronegativity – a rapid access to atomic charges, Tetrahedron 36 (1980) 3219–3228.
[33] A.C. Wallace, R.A. Laskowski, J.M. Thornton, LIGPLOT: a program to generate schematic diagrams of protein-ligand interactions, Protein Engineering 8 (1995) 127–134.
[34] S.B. Needleman, C.D. Wunsch, A general method applicable to the search for similarities in the amino acid sequence of two proteins, Journal of Molecular Biology 48 (1970) 443–453.
[35] M.J. Sippl, Recognition of errors in three-dimensional structures of proteins, Proteins 17 (1993) 355–362.
[36] M. Wiederstein, M.J. Sippl, ProSA-web: interactive web service for the recognition of errors in three-dimensional structures of proteins, Nucleic Acids Research 35 (2007) W407–W410.
[37] P. Gouet, E. Courcelle, D.I. Stuart, F. Metoz, ESPript: analysis of multiple sequence alignments in PostScript, Bioinformatics 15 (1999) 305–308.
[38] J. Kyte, R.F. Doolittle, A simple method for displaying the hydropathic character of a protein, Journal of Molecular Biology 157 (1982) 105–132.
[39] G. Picariello, P. Ferranti, G. Mamone, P. Roepstorff, F. Addeo, Identification of N-linked glycoproteins in human milk by hydrophilic interaction liquid chromatography and mass spectrometry, Proteomics 8 (2008) 3833–3847.
[40] P. Pribble, M.J. Edelman, EC145: a novel targeted agent for adenocarcinoma of the lung, Expert Opinion on Investigational Drugs 21 (2012) 755–761.
[41] K. Simons, D. Toomre, Lipid rafts and signal transduction, Nature Reviews. Molecular Cell Biology 1 (2000) 31–39.
[42] A.L. Jackman, D.S. Theti, D.D. Gibbs, Antifolates targeted specifically to the folate receptor, Advanced Drug Delivery Reviews 56 (2004) 1111–1125.
[43] A. Raval, S. Piana, M.P. Eastwood, R.O. Dror, D.E. Shaw, Refinement of protein structure homology models via long, all-atom molecular dynamics simulations, Proteins 80 (2012) 2071–2079.
[44] J.L. Arolas, F.X. Aviles, J.Y. Chang, S. Ventura, Folding of small disulfide-rich proteins: clarifying the puzzle, Trends in Biochemical Sciences 31 (2006) 292–301.
[45] S.J. de Vries, A.S. Melquiond, P.L. Kastritis, E. Karaca, A. Bordogna, M. van Dijk, J.P. Rodrigues, A.M. Bonvin, Strengths and weaknesses of data-driven docking in critical assessment of prediction of interactions, Proteins 78 (2010) 3242–3249.
[46] O.F. Lange, D. van der Spoel, B.L. de Groot, Scrutinizing molecular mechanics force fields on the submicrosecond timescale with NMR data, Biophysical Journal 99 (2010) 647–655.
[47] D.J. O'Shannessy, E.B. Somers, E. Albone, X. Cheng, Y.C. Park, B.E. Tomkowicz, Y. Hamuro, T.O. Kohl, T.M. Forsyth, R. Smale, Y.S. Fu, N.C. Nicolaides, Characterization of the human folate receptor alpha via novel antibody-based probes, Oncotarget 2 (2011) 1227–1243.
[48] R.B. Orr, B.A. Kamen, Identification of a point mutation in the folate receptor gene that confers a dominant negative phenotype, Cancer Research 55 (1995) 847–852.
[49] B. Vaitilingam, V. Chelvam, S.A. Kularatne, S. Poh, W. Ayala-Lopez, P.S. Low, A folate receptor-alpha-specific ligand that targets cancer tissue and not sites of inflammation, Journal of Nuclear Medicine 53 (2012) 1127–1134.
[50] E.F. Pettersen, T.D. Goddard, C.C. Huang, G.S. Couch, D.M. Greenblatt, E.C. Meng, T.E. Ferrin, UCSF Chimera – a visualization system for exploratory research and analysis, Journal of Computational Chemistry 25 (2004) 1605–1612.